ChemComm

Accepted Manuscript

This article can be cited before page numbers have been issued, to do this please use: P. S. Mukherjee, B. Gole and U. Sanyal, *Chem. Commun.*, 2015, DOI: 10.1039/C4CC09228G.

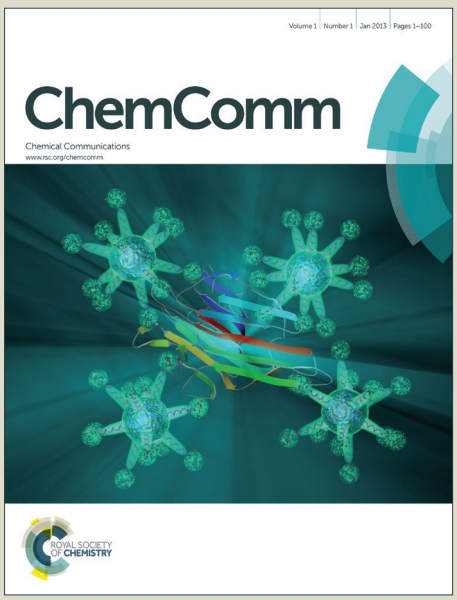

ROYAL SOCIETY OF CHEMISTRY

www.rsc.org/chemcomm

View Article Online
DOI: 10.1039/C4CC09228G

Journal Name

RSCPublishing

COMMUNICATION

A smart approach to achieve exceptionally high loading of metal nanoparticles supported by functionalized extended frameworks for efficient catalysis

Cite this: DOI: 10.1039/x0xx00000x

Received 00th January 2012,
Accepted 00th January 2012

DOI: 10.1039/x0xx00000x

www.rsc.org/

Bappaditya Gole,[a] Udishnu Sanyal[a] and Partha Sarathi Mukherjee*[a]

The problem associated with metal nanoparticles (NPs) agglomeration when tried to achieve high loading amount has been solved by a new way of functionalization of MOFs' pores with terminal alkyne moieties. The alkynophilicity of the Au^{3+} ions has been utilized successfully for exceptional high loading (~50 wt %) of Au-NPs on supported functionalized MOFs.

"Metal nanoparticles @ MOFs" composites are a promising class of materials due to various fascinating properties of both the parent components that composites possess. Such fascinating properties of the components make the composites very potential for various applications especially in the field of heterogeneous catalysis.[1] Advantage of using MOFs as the host materials and/or stabilizing agents for the NPs over the other porous materials can be elucidated to their rationally designed framework structure, tunable pore size on the order of molecular dimensions and chemical tailoring of the inner surface of the channels and cavities.[2] Such tunable cavities control the nucleation, growth of the particles, particle size, and size distribution. Moreover, they also provide confined space for the catalyzed reactions to take place with enhanced activity and better selectivity.[3]

Loading of metal nanoparticles (MNPs) supported by porous MOFs is realized by two general synthetic approaches.[4] The first and most widely used one is to immobilize metal nanoparticles using MOFs as the host materials wherein a suitable metal precursor is initially loaded inside the cavity followed by subsequent decomposition or reduction to generate metal atoms which further grow into the nanoparticles.[5] The second and most recent approach is the use of metal NPs as seeds to construct the MOFs structures around it using their precursors.[6] Very recently, "double solvent approach" is reported to prepare the ultrafine Pt-nanoparticles inside MIL-101 without any deposition on the external surface of the host matrices.[7]

Although considerable research efforts have been devoted in this direction, a facile methodology is still essential to provide selective introduction of metal precursors inside the MOFs cavities and control the formation of ultrafine narrow-sized metal nanoparticles with uniform size distribution. Another very important aspect is to enhance loading amount of MNPs, a combination of high loading amount and smaller particle size maximizes the presence of large amount of catalytically active NPs and high surface area respectively, for superior catalytic activity. However, synthesis of MNPs by wet chemical method with uniform distribution and small size was evident from precedent literature with loading amount generally less than 20 wt %, beyond which particles tend to agglomerate.[4a]

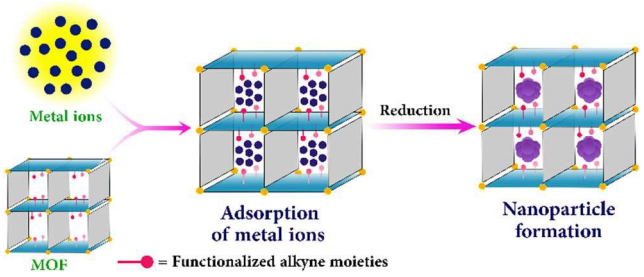

Scheme 1. Schematic illustration of MNPs synthesis.

Functionalization of MOFs' interior could be an ideal approach to achieve high loading with uniform size distribution. Proof-of-concept has been demonstrated herein by reporting the generation of Au-NPs utilizing pre-functionalization of MOFs with terminal alkyne functionality because of well-known alkynophilicity of Au^{3+} ions (Scheme-1). The presence of terminal alkyne moieties initially help to stabilize Au^{3+} ions uniformly throughout the MOF's matrix and subsequently produced MNPs upon reduction. Terminal alkyne group acts as stabilizer to control the growth of the particles and stabilize them in narrow size regime. The loading amount was estimated to be as high as 50 wt % with excellent monodispersity. As mentioned above, due to the problem of agglomeration, such a high loading of nanoparticles on MOF support was never achieved before by wet chemical approach.

Reduction of phenolic nitro compounds, particularly nitrophenol (4-NP), 2,4-dinitrophnol (2,4-DNP) etc., has been recent concern primarily due to their explosive nature as well as their role as severe environment pollutants.[8] On the other hand, their reduced products are quite useful for various applications.[9] The Au-NPs supported MOFs described herein (Au@MOF) were then employed for efficient catalytic reduction of phenolic nitro compounds with $NaBH_4$.Very high efficiency of the Au@MOF catalysts compared to

View Article Online
DOI: 10.1039/C4CC09228G
Journal Name

earlier reports could be accounted for both small particle size as well as extremely high loading amount.

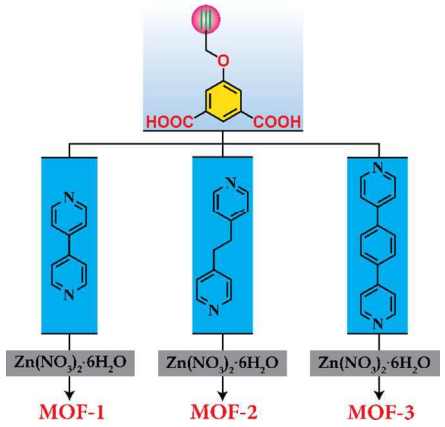

Scheme 2. Schematic representation of preparation of different MOFs depending of the pillar height of the bipyridyl linkers.

Solvothermal reactions of 5-(prop-2-yn-1-yloxy)isophthalic acid (*pip*) and $Zn(NO_3)_2$•$6H_2O$ with various 4,4′-bipyridyl derivatives in *N,N*-dimethylformamide (DMF) at 100 °C for 24 h produced **MOF-1**, **MOF-2** and **MOF-3** having different porosity (Scheme 2). Single-crystal X-ray diffraction analyses of **MOF-1** and **MOF-2** revealed that both the structures are nearly isostructural. In all the frameworks, the dicarboxylic acid moiety of the ligand formed 2D layered networks connecting distorted octahedral Zn^{2+} ions. These 2D layers are interconnected to each other by different pillar linkers via coordination with the axial positions of the Zn^{2+} ions to render 3D MOFs with huge porous channels. Interestingly, as expected the ethynyl moieties are pointed towards the interior of the MOFs' pores. It was observed that in **MOF-1** the ethynyl moieties are present in every channel; however, in **MOF-2**those are located in alternate channels.

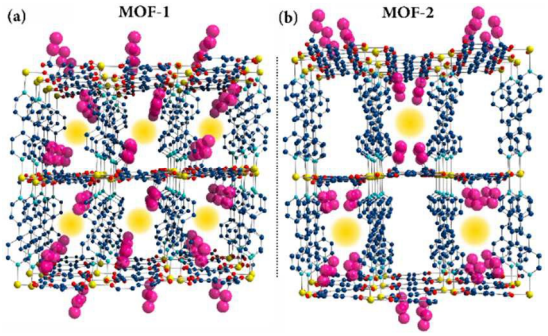

Fig. 1. Crystal structures of **MOF-1** and **MOF-2**. (a) Extended three-dimensional network of **MOF-1** showing channel-like pores. Each pore is decorated with functionalized alkyne moieties. (b) The alternate pores are functionalized with alkyne moieties in **MOF-2**. The alkyne moieties are highlighted in pink color. Color codes: yellow, cyan, navy blue and red represent Zn, N, C and O, respectively.

Solution infiltration technique was adapted to load the metal ions inside the MOFs cavities and subsequent reduction by $NaBH_4$yielded Au-NPs. When methanol solution of $HAuCl_4$ was subjected to activated **MOF-3** crystals, the bright yellow color of the $HAuCl_4$ solution disappeared gradually and concurrently **MOF-3** crystals turned yellow from colorless, which indicated the adsorption of Au^{3+} ions into the MOF (Fig. 2). The adsorption process was significantly facilitated by stabilization of Au-ions inside the MOF's pores owing to the strong Au-ethynyl interaction. The amount of Au^{3+} ions adsorbed into MOF may depend on either increasing the time or increasing $HAuCl_4$ concentration. To get an insight on this adsorption process, scanning electron microscope (SEM)-energy dispersive X-ray (EDAX) mapping was carried out using Au^{3+} adsorbed **MOF-3**. Fig. 2(f) reflects that $HAuCl_4$ was adsorbed homogeneously throughout the entire **MOF-3** crystal. Subsequent reduction of Au^{3+}ions by $NaBH_4$ yielded Au NPs which was indicated by a color change from yellow to purple-red.

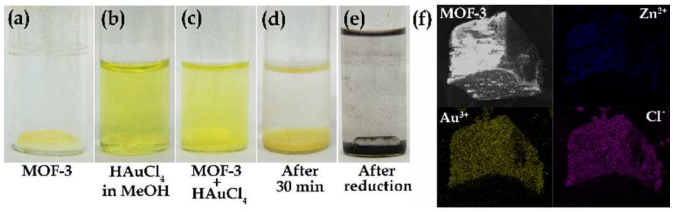

Fig. 2. Two-step formation of Au-NPs. (a) **MOF-3**, (b) $HAuCl_4$ solution in methanol, (c) **MOF-3** and $HAuCl_4$ together, (d) visual color change after 30 min. Supernatant turned colorless from yellow and **MOF-3** crystals turned yellow. (e) Reduction of Au^{3+} ions to Au NPs by $NaBH_4$. (f) SEM-EDAX mapping of $HAuCl_4$ adsorbed **MOF-3**.

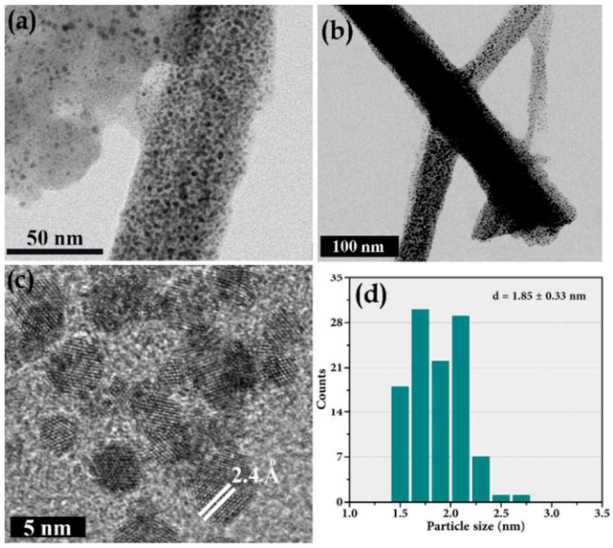

Fig. 3. 50 wt % Au loading in **MOF-3**. (a) Bright-field TEM image showing the Au NPs are homogeneously distributed in **MOF-3**. (b) STEM bright field image of the **Au@MOF-3**. (c) HRTEM image showing lattice spacing (d=2.4 Å) corresponds to (111) plane of fcc Au. (d) Corresponding Au NPs size distribution histogram.

To determine the maximum loading capacity of the MOF without altering monodispersity and particle size of the NPs, the MNPs loading was increased gradually starting from 5 wt % using **MOF-3** until the particles tend to agglomerate. A maximum of 50 wt % Au-NPs loading was realized in this case. This NPs loading amount is unprecedented high wet chemical method using MOF support. Inductively coupled plasma (ICP) analysis demonstrated that the loading amount is 49.3 ± 0.4 wt %. Bright-field TEM image (Fig. 3a) of the samples containing 50 wt % of Au NPs evidenced the formation of uniform nanoparticles with narrow size distribution throughout the MOF-matrix. A similar observation was also noted from (Fig. 3b) the image of the sample obtained from a different area. The size distribution histogram (Fig. 3d) gave an average particle size of 1.85 ± 0.3 nm, which further indicated the monodispersity of the samples. The Au^0 NPs are mainly located

View Article Online
DOI: 10.1039/C4CC09228C COMMUNICATION

inside pore of the **MOF-3** as observed from surface area measurement and pore diameter estimation. The surface area and pore diameter are reduced significantly to 2.195 m^2/g and 0.88 nm from 54.835 m^2/g and 2.77 nm respectively after loading of the 50 wt% Au NPs into **MOF-3**. This is only possible if the pores of the **MOF-3** are blocked by Au^0 NPs. The crystalline nature of the particles was apparent from the HRTEM image which showed lattice fringes with a *d*-spacing of 2.4 Å corresponding to the (111) plane of FCC Au NPs. The preservation of MOFs structure even after loading of Au-NPs has been established by PXRD techniques (Fig. S10). The formation of Au^0 NPs was further confirmed by X-ray photoelectron spectroscopy (XPS). Appearance of doublet (Fig. S10) at 88 eV and 84.4 eV corroborated to two distinct spin-orbit pair $4f_{5/2}$ and $4f_{7/2}$ respectively, corresponding to Au^0. The complete characterization of the samples containing 5 and 20 wt % of Au NPs are provided in the Supporting Information.

To establish whether the alkyne moieties actually have any distinct role to stabilize the Au^{3+} ions or Au-NPs, a structurally similar MOF (**MOF-A**) (see Supporting Information for the detail structural characterization) functionalized with phenyl moiety instead of ethynyl group has been used. Interestingly, loading of only 5 wt % Au-NPs showed that **MOF-A** cannot stabilize either metal ions or the metal NPs. Fig. 4a shows the TEM BF image of **Au@MOF-A** which revealed agglomerated nature of the particles and thus located on the outer surface of **MOF-A** crystal. Alongside agglomerated particles, a few separated spherical particles were also found, however, they are much larger (>12 nm) in size. Both the STEM BF and STEM-HAADF images of the sample also indicated the agglomerated nature of Au-NPs.

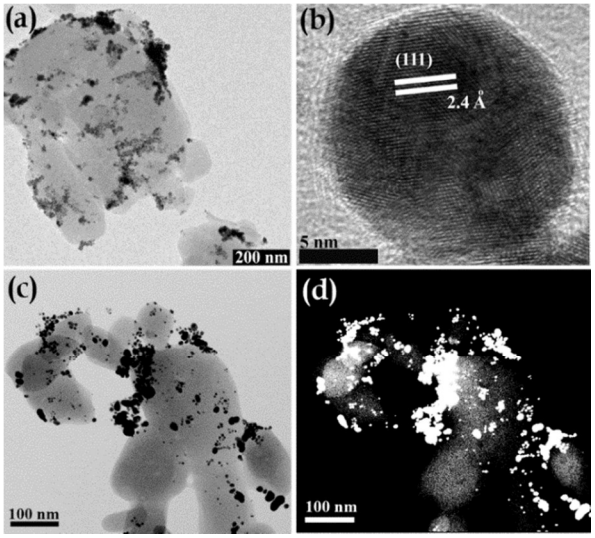

Fig. 4. 5 wt % Au loading in **MOF-A**. (a) Bright-field TEM image showing the Au NPs are mostly agglomerated and located on the surface of **MOF-A**. (b) HRTEM image (c) STEM bright field image and (d) STEM-HAADF image of the **Au@MOF-A**.

Systematic study on the effect of MOF's pore size on metal NPs size is extremely rare. In this current study, both porosity as well as surface area of the MOFs increase from **MOF-1** to **MOF-3** as observed from single crystal X-ray structure depending on the length of dipyridyl pillars. Therefore, to determine the effect of pore sizes of the MOFs, 50 wt % of Au NPs were loaded on the **MOF-1** and **MOF-2**.In contrast to **MOF-3**, less porous **MOF-1** and **MOF-2** yielded average particle size 2.87 ± 0.4 and 2.70 ± 0.9 nm, respectively. The larger particle size observed in these cases compared to MOFs pore size could be rationalized by considering their location outside MOFs cavity, but stabilized with ethynyl moieties.

Table 1. Size of Au NPs on different supported MOFs.

Au@MOFs	Loading amount	Size of NPs (nm)
Au@MOF-1	50 wt %	2.87 ± 0.4
Au@MOF-2	50 wt %	2.70 ± 0.9
Au@MOF-3	50 wt %	1.85 ± 0.3

Reduction of phenolic nitro compounds by aqueous $NaBH_4$ is thermodynamically favorable. But, due to high kinetic barrier those reactions are often extremely slow.[10] The Au-NPs catalyzed these reactions because of the reactive surface Au atoms, which facilitate effective hydrogen transfer from $NaBH_4$ to phenolic nitro compounds. Recently, an intense attention has been devoted to this direction to find effective Au NPs as catalyst in terms of their reactivity and reusability for this purpose. In this regards, we anticipated that our MOFs supported NPs could be the best possible catalyst due to their small size and high loading amount. In a typical experiment, an aqueous solution containing 4-nitrophenol (4-NP) or 2,4-dinitrophenol (2,4-DNP) was mixed with $NaBH_4$ in 3 mL quartz cuvette. The solutions immediately turned bright yellow from light yellow which indicated the formation of phenolate ions. The corresponding absorption peaks at 400 nm and 360 nm for 4-NP and 2,4-DNP respectively, disappeared completely after 60 sec upon addition of **Au@MOFs**. Subsequently, appearance of new absorption peaks at 284 nm and 286 nm confirmed the formation of 4-aminophenol and 2,4-diaminophenol respectively (ESI). The kinetics of the reactions were monitored by time dependent absorbance measurements in every 10 sec at 400 nm and 360 nm for 4-NP and 2,4-DNP, respectively (ESI). Both the reactions were almost completed within 3 min in the presence of **Au@MOFs** which is much faster (Table 2) than the reactions with $NaBH_4$ and $HAuCl_4$ itself (Table S2) and even faster than earlier reports on MOFs supported Au NPs (ESI).[11] Although Au-NPs have different sizes when they were loaded with various MOFs in the present study, the catalytic reactions were too fast to understand whether there was any effect of particle size. Additionally, the catalysts have been reused for several times without much loss of catalytic activity. The stability of the catalysts after catalytic reactions was established by TEM and PXRD technique (ESI). The high monodispersity of NPs clearly indicates the strong interaction between Au and MOFs through the functionalized ethynyl moiety.

Table 2. Estimated rate constants for the Au NPs catalyzed reduction of 4-NP and 2,4-DNP.

Analytes	Rate constant (sec^{-1})		
	Au@MOF-1	Au@MOF-2	Au@MOF-3
NP	6.64×10^{-2}	5.92×10^{-2}	6.88×10^{-2}
2,4-DNP	2.99×10^{-2}	2.46×10^{-2}	2.90×10^{-2}

To generalize whether these catalysts can be used for reduction of other aromatic nitro compounds in the presence of $NaBH_4$, we selected a few other nitro compounds for reduction process in EtOH (due to their insolubility in water). To our surprise, analogous reduction in presence of 2-3 equivalents of $NaBH_4$ and 5 mg (0.6 mol %) of Au@MOFs yielded corresponding azo compounds instead of expected amines (Table 3). More importantly, catalytic reduction of 4–nitrophenol (4-NP) in the presence of **Au@MOF-3** in EtOH also yielded corresponding azo compound, though the same reaction in aqueous medium yielded 4-aminophenol. A control experiment with only $NaBH_4$ did not produce either corresponding amine or azo compound. The detail mechanistic investigations via time dependent ^{1}H-NMR spectroscopy indicated that Au@MOFs

View Article Online
DOI: 10.1039/C4CC09228G
Journal Name

catalyzed reduction in water is extremely fast, which resulted completely reduced product (amine), however, in ethanol the reduction process is slow enough to produce the coupling product (azo). Initially, nitrobenzene reduced to nitrosobenzene (rate constant; k_1), which further reduced to aniline (k_2). In ethanol, the rate of second reduction is slower ($k_1 > k_2$) which resulted in the accumulation of nitroso intermediate. Thus, amine compound produced in the reaction further reacted with nitroso intermediate to yield azo product through water elimination (see ESI). In the presence of only $NaBH_4$, the formation of nitroso is extremely slow compared to **Au@MOF-3** catalyzed reaction and the second reduction to amine is almost negligible as observed from the ^{1}H-NMR spectroscopy (Fig. S22). This control experiment showed that the direct involvement of the Au-NPs into the catalytic process. When the **Au@MOFs** catalytic reductions of 4-NP and 2,4-DNP were carried out in water, the second reduction process is expected to be much faster than the first reduction due to the higher dissociation of $NaBH_4$ in water compared to ethanol. Therefore, in water the reduced product is exclusively amine and also the conversion rate is extremely fast.

Table 3. Au@MOF-3 catalyzed conversion of aromatic nitro to the corresponding azo-derivatives.

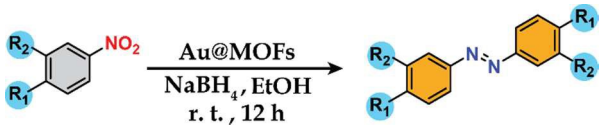

Entry	Reactant (R1, R2)	Product (R1, R2)	Yield (%)
1	H, H	H, H	78
2	Me, H	Me, H	67
3	OMe, H	OMe, H	85
4	OH, H	OH, H	56
5	Br, H	Br, H	83
6	CO_2Me, H	CO_2Me, H	85
7	H, Ph	H, Ph	92

In conclusions, loading of exceptionally large amount of MNPs into MOFs without altering monodispersity and particle size has been successfully achieved by clever functionalization of pores of MOFs. The alkyne functionalized MOFs have been utilized for stabilization of exceptionally large amount of Au-NPs (~50 wt %) by taking advantage of distinct π-donation and π-acceptor characteristics of alkyne functionalities with Au^{3+} ions. The stepwise formation of NPs i.e. adsorption of metal ions inside MOFs and subsequent reduction to NPs was monitored by direct SEM-EDAX mapping and TEM analysis, respectively. These MOFs supported Au-NPs (Au@MOFs) were further employed as efficient heterogeneous catalysts for reduction of 4-NP and 2,4-DNP in the presence of $NaBH_4$ and water as solvent. The catalytic activity obtained in our case is much superior compared to other supported Au-NPs as catalysts reported earlier. The mechanism of completely different reduction behavior of aromatic nitro compounds in ethanol has been investigated by time dependent ^{1}H-NMR spectroscopy. This promising new concept of introducing terminal alkyne into is expected to be very useful for the development of superior catalysts.

PSM is grateful to the DST, India for financial support.

Notes and references

[a]*Department of Inorganic and Physical Chemistry, Indian Institute of Science, Bangalore, India. Fax: (+91)80-2360-1552; Tel: (+91)80-2293-3352; E-mail: psm@ipc.iisc.ernet.in*

Electronic Supplementary Information (ESI) available: Materials, general synthesis procedure, characterization, crystallographic data, detailed catalysis procedure, detailed mechanistic investigations. See DOI: 10.1039/c000000x/

1 (a) K. J. Klabunde and Richards, R. M., in *Nanoscale Materials in Chemistry*, John Wiley & Sons, Inc., 2009, pp. 771; (b) A. Dhakshinamoorthy and H. Garcia, *Chem. Soc. Rev.,* 2012, **41**, 5262; (c) M. O'Keeffe and O. M. Yaghi, *Chem. Rev.,* 2011, **112**, 675; (d) M. Zhao, K. Deng, L. He, Y. Liu, G. Li, H. Zhao and Z. Tang, *J. Am. Chem. Soc.,* 2014, **136**, 1738; (e) G. Li, H. Kobayashi, J. M. Taylor, R. Ikeda, Y. Kubota, K. Kato, M. Takata, T. Yamamoto, S. Toh, S. Matsumura and H. Kitagawa, *Nat. Mater.,* 2014, **13**, 802.

2 (a) S. Kitagawa, R. Kitaura and S.-i. Noro, *Angew. Chem. Int. Ed.,* 2004, **43**, 2334; (b) J.-R. Li, J. Sculley and H.-C. Zhou, *Chem. Rev.,* 2011, **112**, 869; (c) J. R. Long and O. M. Yaghi, *Chem. Soc. Rev.,* 2009, **38**, 1213.

3 (a) K. Na, K. M. Choi, O. M. Yaghi and G. A. Somorjai, *Nano Letters,* 2014, **14**, 5979; (b) C.-H. Kuo, Y. Tang, L.-Y. Chou, B. T. Sneed, C. N. Brodsky, Z. Zhao and C.-K. Tsung, *J. Am. Chem. Soc.,* 2012, **134**, 14345; (c) W. Zhang, G. Lu, C. Cui, Y. Liu, S. Li, W. Yan, C. Xing, Y. R. Chi, Y. Yang and F. Huo, *Adv. Mater.,* 2014, **26**, 4056; (d) P. Pachfule, M. K. Panda, S. Kandambeth, S. M. Shivaprasad, D. D. Diaz and R. Banerjee, *J. Mater. Chem. A*, 2014, **2**, 7944; (e) P. Pachfule, S. Kandambeth, D. D. Diaz and R. Banerjee, *Chem. Commun.* 2014, **50**, 3169.

4 (a) M. Meilikhov, K. Yusenko, D. Esken, S. Turner, G. Van Tendeloo and R. A. Fischer, *Eur. J. Inorg. Chem.,* 2010, **2010**, 3701; (b) A. Aijaz and Q. Xu, *J. Phys. Chem. Lett.,* 2014, **5**, 1400.

5 (a) S. Hermes, M.-K. Schröter, R. Schmid, L. Khodeir, M. Muhler, A. Tissler, R. W. Fischer and R. A. Fischer, *Angew. Chem. Int. Ed.,* 2005, **44**, 6237; (b) T. Ishida, M. Nagaoka, T. Akita and M. Haruta, *Chem. Eur. J.,* 2008, **14**, 8456; (c) H.-L. Jiang, Q.-P. Lin, T. Akita, B. Liu, H. Ohashi, H. Oji, T. Honma, T. Takei, M. Haruta and Q. Xu, *Chem. Eur. J.,* 2011, **17**, 78; (d) D. Esken, S. Turner, O. I. Lebedev, G. Van Tendeloo and R. A. Fischer, *Chem. Mater.,* 2010, **22**, 6393; (e) H.-L. Jiang, B. Liu, T. Akita, M. Haruta, H. Sakurai and Q. Xu, *J. Am. Chem. Soc.,* 2009, **131**, 11302; (f) F. Schröder, D. Esken, M. Cokoja, M. W. E. van den Berg, O. I. Lebedev, G. Van Tendeloo, B. Walaszek, G. Buntkowsky, H.-H. Limbach, B. Chaudret and R. A. Fischer, *J. Am. Chem. Soc.,* 2008, **130**, 6119.

6 G. Lu, S. Li, Z. Guo, O. K. Farha, B. G. Hauser, X. Qi, Y. Wang, X. Wang, S. Han, X. Liu, J. S. DuChene, H. Zhang, Q. Zhang, X. Chen, J. Ma, S. C. J. Loo, W. D. Wei, Y. Yang, J. T. Hupp and F. Huo, *Nat. Chem.,* 2012, **4**, 310.

7 A. Aijaz, A. Karkamkar, Y. J. Choi, N. Tsumori, E. Rönnebro, T. Autrey, H. Shioyama and Q. Xu, *J. Am. Chem. Soc.,* 2012, **134**, 13926.

8 S. J. Toal and W. C. Trogler, *J. Mater. Chem.,* 2006, **16**, 2871.

9 (a) Z. Zhang, C. Shao, P. Zou, P. Zhang, M. Zhang, J. Mu, Z. Guo, X. Li, C. Wang and Y. Liu, *Chem. Commun.,* 2011, **47**, 3906; (b) A. Gangula, R. Podila, R. M, L. Karanam, C. Janardhana and A. M. Rao, *Langmuir,* 2011, **27**, 15268; (c) H. Xu, X. Chen, J. Gao, J. Lin, M. Addicoat, S. Irle and D. Jiang, *Chem. Commun.* 2014, **50**, 1292.

10 Z. D. Pozun, S. E. Rodenbusch, E. Keller, K. Tran, W. Tang, K. J. Stevenson and G. Henkelman, *J. Phys. Chem. C,* 2013, **117**, 7598.

11 (a) F. Ke, J. Zhu, L.-G. Qiu and X. Jiang, *Chem. Commun.,* 2013, **49**, 1267; (b) H.-L. Jiang, T. Akita, T. Ishida, M. Haruta and Q. Xu, *J. Am. Chem. Soc.,* 2011, **133**, 1304.